Int. J. Electrochem. Sci., 13 **(2018)** 9333 – 9345, doi: 10.20964/2018.10.53

International Journal of
ELECTROCHEMICAL
SCIENCE
www.electrochemsci.org

A Molecularly Imprinted Polythionine-Modified Electrode Based on a Graphene-Gold Nanoparticle Composite (MIP/AuNPs/rGO/GCE) for the Determination of Thrombin

Shaoming Yang Jie Yang, Qiang Cao, Yue Zheng, Chaopeng Bai, Yu Teng, and Wenyuan Xu**

School of Materials Science and Engineering, East China Jiaotong University, Nanchang 330013, Jiangxi, China
*E-mail: yangsm79@163.com, xwy1027@sina.com

Received: 16 May 2018 / *Accepted:* 7 August 2018 / *Published:* 1 September 2018

A novel electrochemical sensor for the detection of thrombin (THR) was fabricated based on a glassy carbon electrode by the modification of molecularly imprinted polymers (MIP) and nanocomposites of graphene and gold nanoparticles. A MIP polythionine (PTH) film was formed by cyclic voltammetric electropolymerization and took the role of the redox probe to explore the sensor performance. Nanocomposites for the purpose of enhancing the sensitivity were characterized with SEM and energy dispersive spectroscopy. The stepwise preparation process of the MIP sensor was monitored with cyclic voltammetry and electrochemical impedance spectroscopy. After the experiments to determine the optimal conditions, the performance of the sensor was investigated. A linear relationship between the peak current of the PTH redox probe and the logarithm of the THR concentration was obtained over the range of 1.0×10^{-8} g/L~1.0×10^{-5} g/L with a detection limit of 1.0×10^{-9} g/L. In comparison with the non-molecularly imprinted sensor, the MIP sensor showed good anti-interference ability and high selectivity.

Keywords: Molecularly imprinted polymer · Polythionine · Nanocomposites · Sensor · Thrombin

1. INTRODUCTION

A molecularly imprinted electrochemical sensor (MIECS), which integrated the significant advantages of molecularly imprinted polymers (MIP) and electrochemical sensors, exhibits specific features such as high sensitivity and selectivity, chemical and mechanical stability, reusability, ease of preparation, and low cost [1,2]. Hence, MIECSs have aroused extensive attention and have been successfully applied to recognize and detect different molecules, including dopamine [3], acetaminophen [4], methyl parathion [5], bisphenol A [6] and proteins, such as hemoglobin [7] and

bovine serum albumin [8]. However, the molecular imprinting of proteins is still a challenge due to the unstable three-dimensional conformation of proteins in the harsh imprinting conditions and difficulty in eluting target proteins with a large molecular size from the imprinted cavities. Surface imprinting has emerged as the most effective macromolecule imprinting method. This approach imprints local binding sites at or close to the surface of the MIP, which overcomes the above problems that occurred during protein imprinting [9].

Among the many types of surface imprinting methods, electropolymerization is a potential technique for developing MIECSs used for protein recognition and detection because of its advantages of easy preparation, simple control of the MIP layer thickness, good stability and good reproducibility. Although various monomers such as pyrrole [10], *o*-phenylenediamine [11], and dopamine [12] have been electropolymerized to form MIPs on the surface of the base electrode for protein detection, the presence of the electroactive probe $[Fe(CN)_6]^{3-}$ in the solution was necessary for the measurement of the current signal before and after the incubation of the target protein. The monomer thionine (TH) can also be electropolymerized to form stable and electroactive poly(thionine) (PTH). PTH, acting as both an excellent electron mediator and immobilization matrix, has been extensively applied for biosensing applications of glucose [13], hydrogen peroxide [14], NADH [15] and DNA [16]. Based on this idea, this paper proposed a new project, in which the electropolymerized PTH film can serve two roles: a MIP film for target recognition and an electroactive probe for the measurement of the signal change after the binding of the target.

In the reported literature regarding MIP sensors for protein detection, nanomaterials such as graphene and gold nanoparticles, possessing some key features such as a large surface area, good biocompatability and excellent conductivity, were introduced into the preparation of MIP sensors as the supporting material, which enhanced the sensitivity and amplified the signal response of the sensors [17, 18]. The nanocomposites of graphene-gold nanoparticles offer a better microenvironment for protein binding and better electrochemical properties due to the synergistic effect [12, 19].

Herein, thrombin (THR) was selected as the target protein to explore the viability of the proposed MIECS method based on the nanocomposites of graphene-gold nanoparticles, in which PTH serves two roles as the MIP film and electroactive probe. Thrombin is a serine proteolytic hydrolase that is widely found in the mammalian blood clotting system and can catalyze fibrinogen to fibrin. It plays a significant role in wound healing, inflammation, and blood coagulation [20, 21]. The concentration of THR is an important indicator to measure whether the coagulation mechanism is healthy.

In this work, THR and TH were considered as the protein template and monomer, respectively. The merits of nanocomposites and electropolymerization were fully utilized to successfully construct a sensitive and selective MIECS based on surface imprinting. TH was electropolymerized in the presence of THR on the surface of a glassy carbon electrode (GCE), which was first modified with nanocomposites of graphene-gold nanoparticles to enhance the sensitivity of the proposed sensor. The electropolymerized PTH played two roles here, as the MIP film and electroactive probe, thus simplifying the preparation process of the MIP sensor and requiring no external electroactive probe of $[Fe(CN)_6]^{3-}$. The target THR was determined through the reduction signal decrease of PTH due to the electrochemical inertness of THR depressing the electron transfer of PTH on the electrode surface. The

reduction signal produced by PTH has a linear relationship with the concentration of THR. The results exhibited a wide detection range, high selectivity, high sensitivity, and good reproducibility.

2. EXPERIMENTAL

2.1 Chemicals and reagents

$HAuCl_4$ was purchased from Sigma-Aldrich. Graphite was from the Shantou Xilong Chemical Company. Thrombin (THR, M_w = 36700 g/mol, ≥200 U/mg) was obtained from the Bomei Biotechnology Company (Shanghai, China). Thionine was obtained from the Shanghai Chemical Reagent Company. Glucose oxidase (GOD, ≥100 U/mg) was from the Shanghai Biological Engineering Company. Horseradish peroxidase (HRP, ≥250 U/mg) was purchased from the Shanghai Sanjie Biological Co., Ltd. Bovine serum albumin (BSA) was from the Shanghai Crystal Pure Co., Ltd, and dopamine hydrochloride (DPA) was obtained from Aladdin (Shanghai, China).

2.2 Instruments

Scanning electron microscopy (SEM) tests were implemented on a JSM-6701F JEOL SEM. All electrochemical measurements were performed on a CHI660C electrochemical workstation (Shanghai, China) with a common three-electrode system, which consisted of the modified GCE as the working electrode, a platinum wire as the auxiliary electrode and a Ag/AgCl electrode as the reference electrode.

2.3 Preparation of the MIP sensor and NIP sensor

Before modification, the glassy carbon electrode was pretreated according to reference 22. Graphene oxide (GO) was prepared by the modified Hummers method [23]. Five milligrams of GO was dispersed in 10 mL of distilled water under ultrasonic vibration for 1 h to obtain a GO dispersion. Six microliters of GO dispersion was dropped onto the pretreated GCE and allowed to dry. Then, GO was electrochemically reduced in a 0.1 M KCl solution by cyclic voltammetry over the range of -1.7 V~0.2 V for 20 cycles with a scan rate of 100 mV/s. After the electrochemical reduction of GO, a reduced graphene oxide (rGO)-modified GCE (rGO/GCE) was acquired. Next, the prepared rGO/GCE was immersed in a 2 mM $HAuCl_4$ solution, followed by cyclic voltammetry for 26 segments at a rate of 100 mV/s over the range of +1.4 V~-0.2 V to obtain a gold nanoparticle (AuNPs)-modified rGO/GCE (AuNPs/rGO/GCE).

The AuNPs/rGO/GCE was first anodized at +1.5 V for 660 s in PBS (pH = 6.4) containing 0.04 mg/mL THR and 2 mM TH. Then, the electropolymerization was implemented by a cyclic voltammetry (CV) method at a rate of 100 mV/s for 120 segments between +0.1 V and -0.4 V to give a polymer-modified AuNPs/rGO/GCE. Next, the polymer-modified AuNPs/rGO/GCE was eluted for 20 min in acetate-buffered solution (ABS, pH = 4.6) to remove the THR molecule, and a molecularly imprinted sensor for THR recognition (denoted as MIP/AuNPs/rGO/GCE) was obtained.

As a control, a nonimprinted sensor (denoted as NIP/AuNPs/rGO/GCE) was prepared by the

same procedure except for the absence of THR template molecules in the polymerization process.

2.4 Electrochemical measurements

The cyclic voltammetry was carried out in the range of from 0.2 V to -0.6 V in phosphate buffer (pH = 6.0) containing 0.1 M NaCl. The electrochemical impedance spectroscopy (EIS) was carried out in the solution of 5 mmol/L $K_3[Fe(CN)_6]/K_4[Fe(CN)_6]$ (V:V = 1:1) over a frequency range from 1 to 100 000 Hz with an amplitude of 5 mV and was simulated by ZSimpWin software. Differential pulse voltammetry (DPV) was achieved over the range of 0 V to -0.4 V in phosphate buffer containing 0.1 M NaCl.

3. RESULTS AND DISCUSSION

3.1 SEM and EDS characterization of the nanocomposite-modified electrode

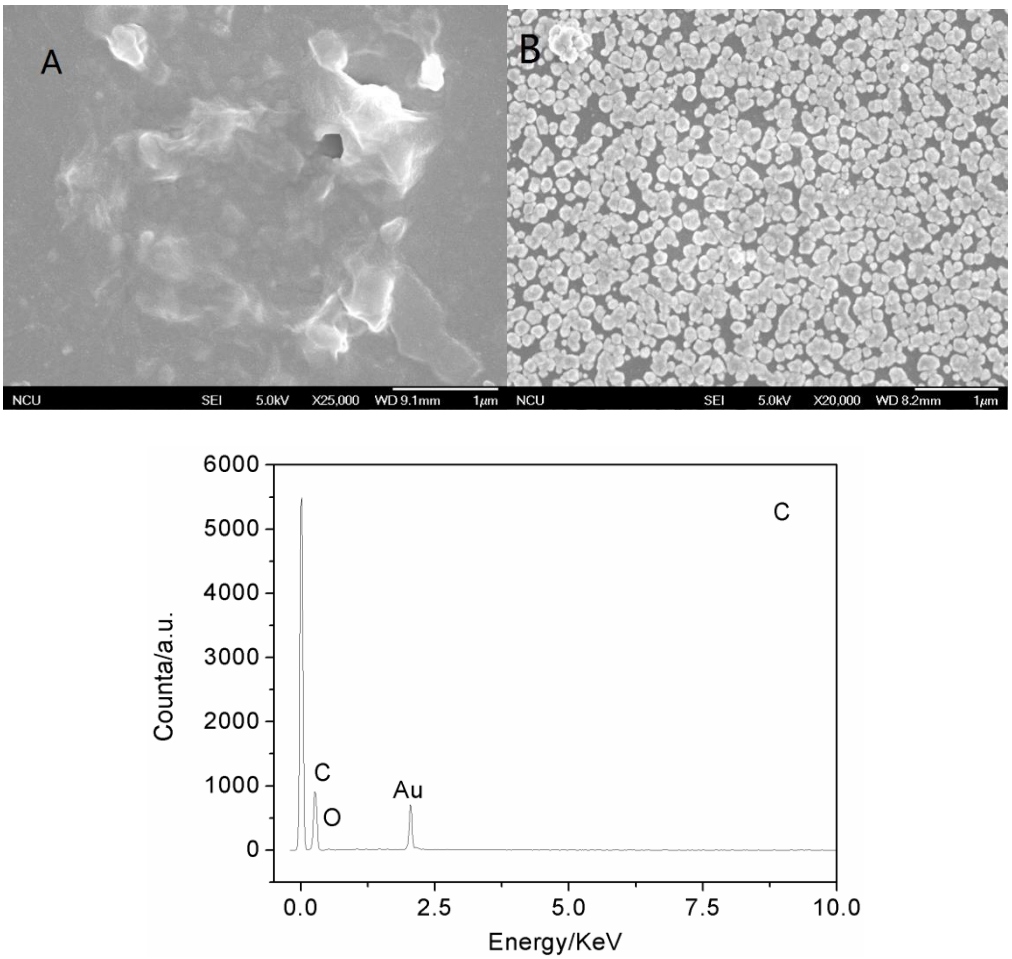

Figure 1. (A) SEM image of the rGO/GCE; (B) SEM image of AuNPs/rGO/GCE; and (C) EDS image of AuNPs/rGO/GCE.

SEM was employed to analyze the surface morphologies of the rGO/GCE and AuNPs/rGO/GCE. As shown in Fig. 1 (A), it can be seen that many thin wrinkles are observed on the surface of the electrode, which was also observed in reference 24 for the SEM of rGO, indicating that the rGO obtained by electrochemical reduction is immobilized on the surface of the GCE. Fig. 1 (B) is the image of the AuNPs/rGO/GCE, and it can be seen that particles of approximately 70~100 nm are evenly distributed on the surface of the modified electrode. Fig. 1 (C) shows an energy spectrum analysis of the modified electrode. The peaks of C and Au elements can be seen from the image, indicating that AuNPs/rGO is successfully immobilized onto the electrode surface.

3.2 Cyclic voltammetric characterization of different modified electrodes

The stepwise preparation process of the sensor was characterized by cyclic voltammetry in PBS (pH = 6.0, 0.1 M NaCl) at a rate of 100 mV/s over the range from +0.2 V to -0.6 V. The cyclic voltammetry responses of the different electrodes are shown in Fig. 2 (A). The curves a, b, c, d and e are denoted GCE, rGO/GCE, AuNPs/rGO/GCE, MIP/AuNPs/rGO/GCE before template extraction and MIP/AuNPs/rGO/GCE after template extraction, respectively. It can be seen that the bare GCE has no redox peak in the range of 0.2 V to -0.6 V, and the charging current of the electrode becomes larger due to the modification with rGO and AuNPs. After the molecularly imprinted film was electropolymerized, a pair of redox peaks appeared ca. -0.2 V, indicative of the redox peak of PTH [25]. After the template was eluted, the peak current of PTH obviously increased because cavities formed by the template extraction facilitated the electron transfer between PTH and GCE.

To demonstrate the roles of AuNPs and rGO, a MIP/GCE was prepared. As shown in Fig. 2 (B), the peak current of the MIP/AuNPs/rGO/GCE was much higher than that of MIP/GCE, which proved that the nanoparticles of AuNPs and rGO effectively increase the specific surface area and promote the electron transfer [26].

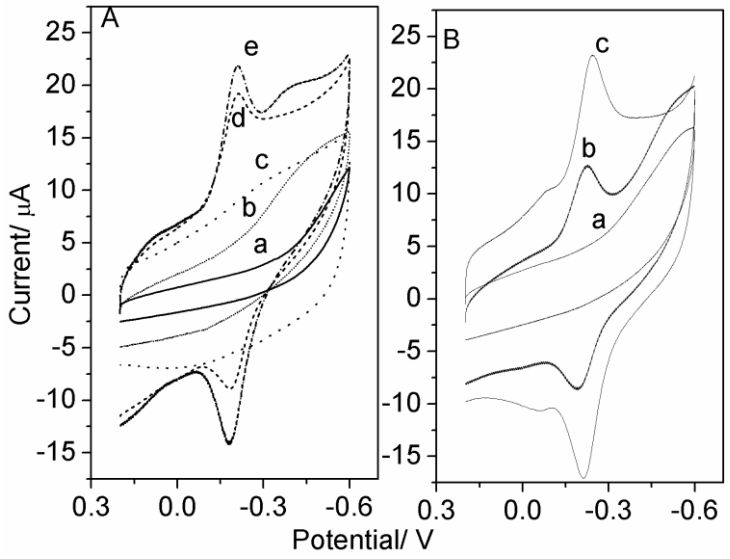

Figure 2. (A) CV responses of the (a) bare GCE, (b) rGO/GCE, (c) AuNPs/rGO/GCE, (d) MIP/AuNPs/rGO/GCE before template extraction, and (e) MIP/AuNPs/rGO/GCE after template extraction in PBS (pH = 6.0, 0.1 M NaCl). (B) CV responses of the (a) GCE, (b) MIP/GCE, and (c) MIP/AuNPs/rGO/GCE in PBS (pH = 6.0, 0.1 M NaCl).

The NIP/AuNPs/rGO/GCE was also characterized by cyclic voltammetry, as shown in Fig. 3. The curves a, b and c represent the GCE as well as the NIP/AuNPs/rGO/GCE before and after template extraction, respectively. Although there is a pair of redox peak of PTH ca. -0.2 V in curve b, no marked change was found for the NIP/AuNPs/rGO/GCE after template extraction in curve c, indicating that there was no cavity formed on the nonimprinted film to enhance electron transfer between PTH and the GCE [27].

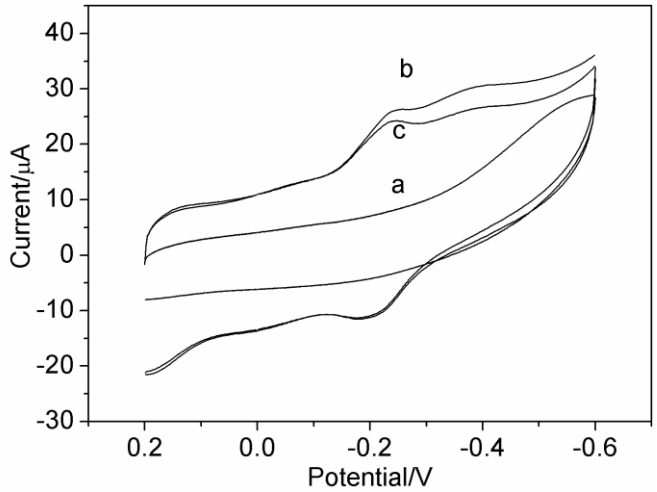

Figure 3. CV responses of the (a) bare GCE, (b) NIP/AuNPs/rGO/GCE before template extraction, and (c) NIP/AuNPs/rGO/GCE after template extraction in PBS (pH = 6.0, 0.1 M NaCl).

3.3 Electrochemical impedance spectroscopy (EIS) characterization of different modified electrodes

EIS can clearly characterize the impedance change of the modified electrode surface. The impedance spectra consist of a semicircle portion in the high-frequency regions and a linear portion in the low-frequency regions. The diameter of the semicircle section represents the electron transfer resistance R_{ct}, while the straight line represents the diffusion controlled process [28]. Fig. 4 shows the electrochemical impedance spectra of the modified electrode in 5 mM $K_3[Fe(CN)_6]/K_4[Fe(CN)_6]$ solution containing 0.1 M KCl. The GCE showed a small semicircle (curve a), indicative of the fast electron transfer involved in the electrode reaction. After nanocomposites of rGO and AuNPs were modified on the surface of the GCE, a smaller semicircle was observed (curve b), indicating that the modification with rGO and AuNPs greatly improved the electron transfer rate on the electrode surface [18]. When the MIP film was formed on the AuNPs/rGO/GCE, a significantly increased semicircle was acquired (curve c), indicating that the MIP film and template THR hindered the electron transfer on the electrode. After the template was eluted, a decreased semicircle was observed (curve d) because the removal of the template molecule from the MIP film left some specific recognition cavities, which

facilitated the electron transfer to the electrode surface. Meanwhile, an increase of the semicircle was seen in curve e after the template was recombined with the cavities of the electrode surface, which meant that THR occupied some cavities and blocked the electron transfer [18, 29].

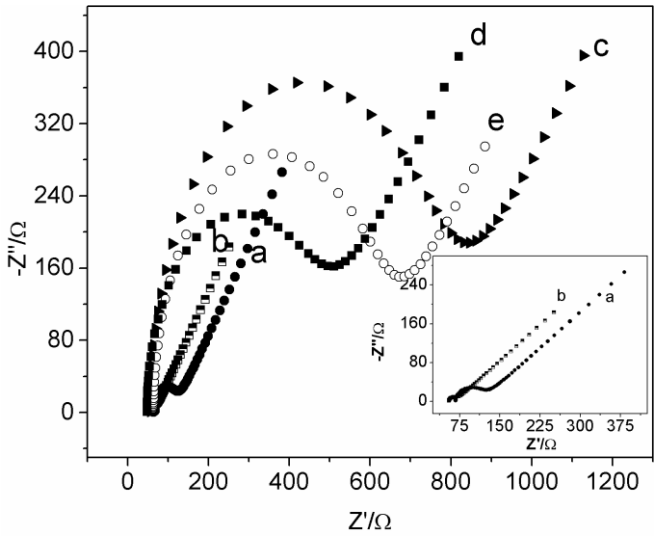

Figure 4. EIS responses of the (a) GCE, (b) AuNPs/rGO/GCE, (c) MIP/AuNPs/rGO/GCE before template extraction, (d) MIP/AuNPs/rGO/GCE after template extraction, and (e) MIP/AuNPs/rGO/GCE after template rebinding.

3.4 Effect of the scan rate on the electrochemical behavior of the MIP sensor

The effect of the scan rate on the peak current of PTH for the MIP/AuNPs/rGO/GCE sensor was investigated, as shown in Fig. 5. In the range of 0.1 V/s~1.0 V/s, the redox peak current increased with the increase of the scan rate. The peak current was linear to the scan rate. The linear equations are I_{pa} (μA) = 0.12-97.00 ν (V/s) (linear correlation coefficient = 0.990) and I_{pc} (μA) = 4.57 + 133.99 ν (V/s) (linear correlation coefficient = 0.992). These results demonstrated that the redox process of PTH in the MIP sensor was controlled by the surface characteristics [30].

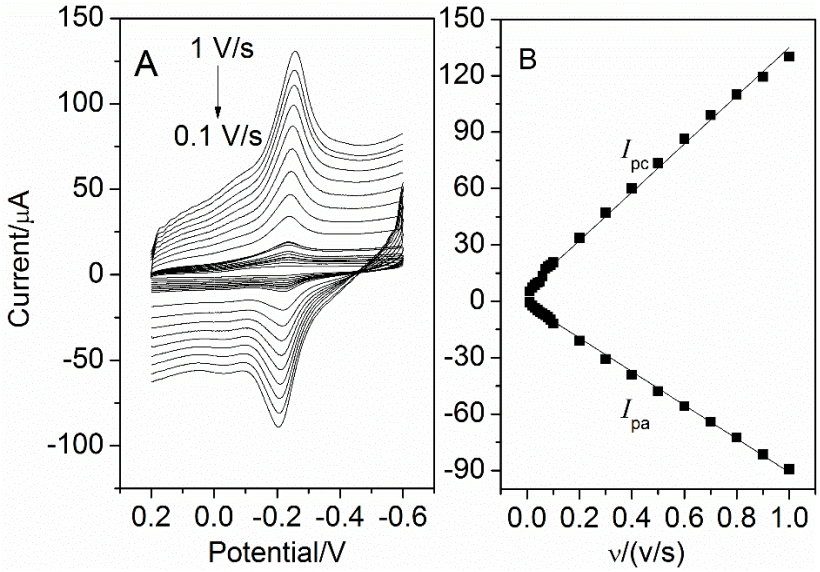

Figure 5. (A) CV responses of the MIP/AuNPs/rGO/GCE with scan rates from 0.1 V/s to 1.0 V/s; (B) linear fitting curve between the peak current and scan rate.

3.5 Optimization of the experimental conditions

The elution efficiency of the template molecule is directly related to the sensitivity of the MIP sensor. ABS (pH = 4.6), 0.1 M NaOH, water and 0.01 M HCl were selected as eluants to elute the template molecules. From Fig. 6 (A), the maximum value of $\Delta I_{elution}$ (defined as $I_{after\ elution}$ minus $I_{before\ elution}$) was obtained for the ABS eluant (pH = 4.6). The reason was that intramolecular hydrogen bonds in the target were destroyed by ABS and so the spatial structure of template was broken down in ABS (pH = 4.6) [31]. Thus, ABS (pH = 4.6) was selected as the eluent.

After selecting ABS (pH = 4.6) as the eluent, the elution time was optimized. The curve in Fig. 6 (B) indicated that the reduction peak signal increased with the increase of the elution time from 5 to 20 min. Beyond the elution time of 20 min, the peak current tended to be stable. Thus, the elution time selected for the subsequent experiments was 20 min.

In addition, other influencing factors including the pH and incubation time were investigated. Overall, the MIP sensor was obtained with the MIP/AuNPs/rGO/GCE in ABS (pH = 4.6) for 20 min to elute the template THR. The prepared MIP sensor was immersed into a PBS supporting solution at a pH of 6.0 containing THR, incubated for 20 min and subsequently measured with the DPV technique.

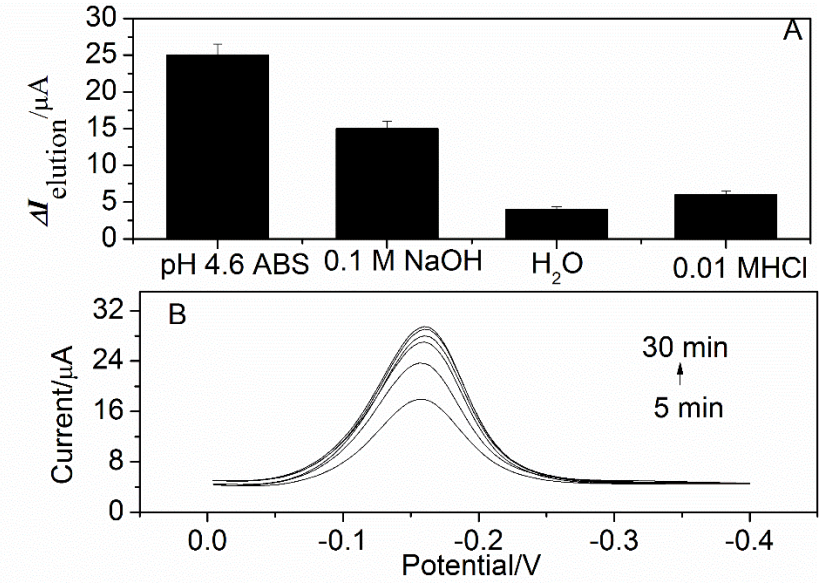

Figure 6. (A) Influence of different elution solutions on responses of the sensor; (B) influence of different elution times on the response of the MIP/AuNPs/rGO/GCE.

3.6 Selectivity, stability and reproducibility of the MIP/AuNPs/rGO/GCE sensor

Bovine serum albumin, diphenylamine, horseradish peroxidase and glucose oxidase were selected as potential interfering substances to evaluate the selectivity of the MIP sensor. The interference was investigated by recording the DPV responses of interfering substances at 10 times the concentration of THR and 5.0×10^{-7} g/L THR in PBS (pH = 6.0). The results are shown in Fig. 7, which demonstrated that there were no noticeable responses from interfering substances. In addition, the NIP sensor had very little current response to both THR and interfering substances. These results showed that the MIP sensor had high selectivity for the template THR.

The MIP sensor was prepared by using the same electrode three times. The current responses were measured for 5.0×10^{-7} g/L THR, and the relative standard deviation was 2.08%. In addition, three MIP sensors were prepared in parallel, and the relative standard deviation obtained for a 5.0×10^{-7} g/L THR measurement was 5.8%. The prepared MIP sensor was stored at 4℃, and the response current was 93.1% of the original current after one week. These results proved that the MIP sensor had good reproducibility and stability.

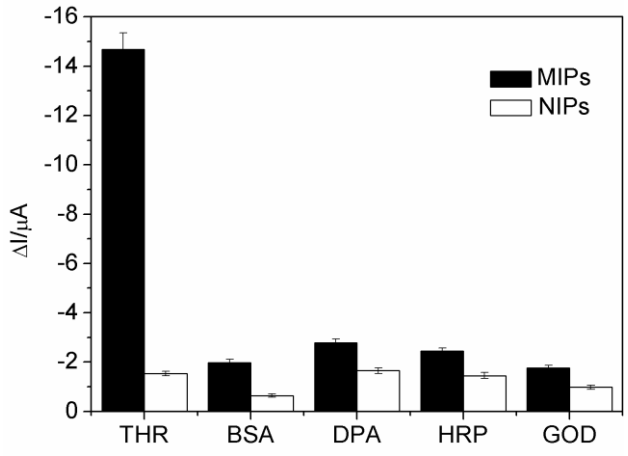

Figure 7. Responses of the MIP/AuNPs/rGO/GCE to different substances.

3.7 Analytical performance of the MIP Sensor

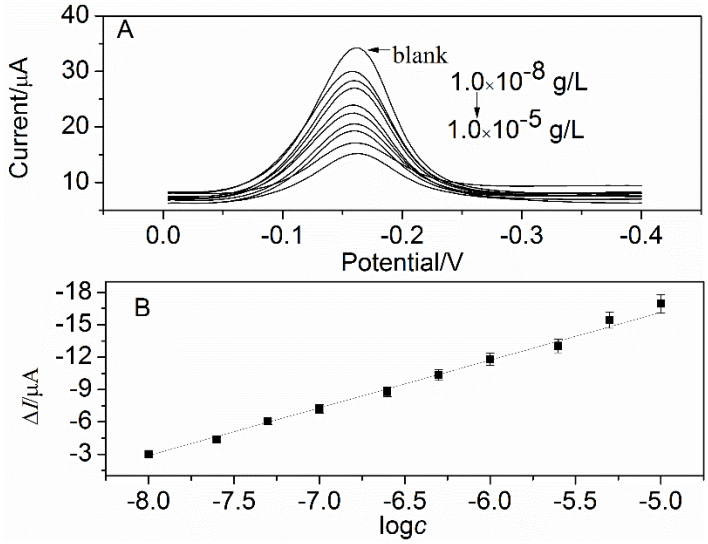

Figure 8. (A) Differential pulse voltammetry responses of the MIP/AuNPs/rGO/GCE sensor to different concentrations of THR; (B) linear fitting curve.

In the optimal experimental conditions, the peak current variation of PTH at the MIP sensor by the DPV technique was measured upon interacting with different concentrations of THR. As shown in Fig. 8, the peak current decreased with the increase of the THR concentration, which was ascribed to the fact that more THR molecules combined with the imprinted sites when the concentration of THR increased, leading to the depression of the electron transfer between PTH and the base electrode, thus resulting in a decrease of the peak current. The peak current variation (ΔI) was found to be linearly related to the logarithm of the THR concentration in the range from 1.0×10^{-8} g/L to 1.0×10^{-5} g/L, as shown in Table 1. The analytical properties of the sensor were compared with those of the literature, including the redox probe, analytical method, linear range, and detection limit. As shown in Table 2,

the proposed sensor showed a low detection limit and comparable linearity, which was ascribed to the excellent electroactive performance of the PTH redox probe and the synergistic effect of rGO and AuNPs.

Table 1 Analytical performance of the sensor for THR

Regression equation	ΔI (μA) = -38.23 - 4.42 log$c$ (g/L)
Linear range	1.0×10^{-8} g/L~1.0×10^{-5} g/L
Detection limit	1.0×10^{-9} g/L
Correlation coefficient (R)	0.995

Table 2. Analytical properties of sensors for the detection of THR

Redox probe	Analytical method	Linear range	Detection limit	Reference
Porphyrin	DPV	5 nmol/L~1500 nmol/L	0.2 nmol/L	32
Polyaniline	DPV	0.1 pmol/L~4 nmol/L	80 fmol/L	33
$[Fe(CN)_6]^{4-/3-}$	EIS	0.3 nmol/L~50 nmol/L	0.01 nmol/L	34
Methylene blue	Square wave voltammetry	2 pmol/L~50 nmol/L	0.97 pmol/L	35
Polythionine	DPV	0.27 pmol/L~0.27 nmol/L	27 fmol/L	This work

To further demonstrate the applicability of the MIP sensor, two different THR samples were prepared in 0.1% bovine serum, and the concentrations of THR were 5.0×10^{-7} g/L and 5.0×10^{-6} g/L, respectively. The recoveries for these two samples by three determinations were 94.3% and 98.6%, respectively, which is indicative of the satisfactory analytical results.

4. CONCLUSIONS

In this work, a novel electrochemical MIP sensor for the detection of THR was fabricated by the MIP film and nanocomposites of rGO and AuNPs modifying the GCE. The nanocomposites of rGO and AuNPs enhanced the sensitivity of the MIP sensor. The MIP film PTH was used as the redox probe for the measurement of the signal change after the binding of THR, thus simplifying the preparation process of the MIP sensor and requiring no external electroactive probe of $[Fe(CN)_6]^{3-}$. The performance of the MIP sensor was tested by CV, DPV and EIS. It can be concluded that the molecularly imprinted sensor prepared by this method exhibited a good linear response in the range of 1.0×10^{-8} g/L ~1.0×10^{-5} g/L for THR with a detection limit of 1.0×10^{-9} g/L (S/N = 3).

ACKNOWLEDGMENTS
This work was financially supported by the National Natural Science Foundation of China (21465012) and the Natural Science Foundation of Jiangxi Province of China (20171BAB203017).

References

1. R. Gui, H. Jin, H. Guo, Z. Wang, *Biosens. Bioelectron.*, 100 (2018) 56.
2. Y. Li, Li Y., M. Hong, Q. Bin, Z. Lin, Z. Lin, Z. Cai, G. Chen, *Biosens. Bioelectron.*, 42 (2013) 612.
3. Y. Liu, J. Liu, J. Liu, W. Gan, B. C. Ye, Y. C. Li, *Microchim. Acta*, 184 (2017) 1285.
4. S. Menon, Jesny S, K. G. Kumar, *Talanta*, 179 (2018) 668.
5. Y. G. Li, J. Liu, Y. Zhang, M. Gu, D. Y. Wang, Y. Y. Dang, B. C. Ye, Y. C. Li, *Biosens. Bioelectron.*, 106 (2018) 71.
6. W. Z. Xu, F. Yuan, C.Y. Li, W. H. Huang, X. Y. Wu, Z. Q. Yin, W. M. Yang, *J. Sep. Sci.*, 39 (2016) 4851.
7. B. Sun, X. Ni, Y. Cao, G. Cao, *Biosens. Bioelectron.*, 19 (2017) 354.
8. M. X. Li, X. H. Wang, L. M. Zhang, X. P. Wei, *Anal. Biochem.*, 530 (2017) 68.
9. X. Kan, Z. Xing, A. Zhu, Z. Zhao, G. Xu, C. Li, H. Zhou, *Sens. Actuators B*, 168 (2012) 395.
10. J. Xia, X. Cao, Z. Wang, Z. Yang, M. Yang, F. Zhang, B. Lu, F. Li, L. Xia, Y. Li, Y. Xia, *Sens. Actuators B*, 225 (2016) 305.
11. N. Karimian, A. P. F. Turner, *Biosens. Bioelectron.*, 59 (2014) 160.
12. X. Shen, Y. Ma, Q. Zeng, J. Huang, J. Tao, L. Wang, *Chemistry Select*, 2 (2017) 6549.
13. M. E. Ghica, C. M. A. Brett, *Talanta*, 130 (2014) 198.
14. S. M. Yang, A. H. Huang, W. L. Zha, Z. P. Wei, L. Z. Zheng, *Acta Chim. Sinica*, 69 (2011) 2143.
15. N. N. Mai, X. Y. Liu, X.D. Zeng, L. Xing, W. Z. Wei, S. L. Luo, *Microchim. Acta*, 168 (2010) 215.
16. M. M. Rahman, N. S. Lopa, Y. J. Kim, D. K. Choi, J. J. Lee, *J. Electrochem. Soc.*, 163 (2016) B153.
17. A. Fatoni, A. Numnuam, P. Kanatharana, W. Limbut, P. Thavarungkul, *Analyst*, 139 (2014) 6160.
18. L. Li, L. Fan, Y. Dai, X. Kan, *Microchim. Acta*, 182 (2015) 2477.
19. G. Li, S. Li, Z. Wang, Y. Xue, C. Dong, J. Zeng, Y. Huang, J. Liang, Z. Zhou, *Anal. Biochem.*, 547 (2018) 37.
20. Q. Zhao, J. Gao, *Chem. Commun.*, 49 (2013) 7720
21. Z. Chen, Y. Tan, C. Zhang, L. Yin, H. Ma, N. Ye, H. Qiang, Y. Lin, *Biosens. Bioelectron.*, 56 (2014) 46
22. S. Yang, L. Li, X. Zhang, P. Shang, S. Ding, W. Zha, W. Xu, *Can. J. Chem.* 95(2017) 799.
23. W. S. Hummers, R. E. Offeman, *J. Am. Chem. Soc.*, 80 (1958) 1339.
24. J. M. Jian, Y. Y. Liu, Y. L. Zhang, X. S. Guo, Q. Cai, *Sensors*, 13 (2013) 13063.
25. S. M. Yang, W. L. Zha, H. Li, Q. Sun, B. Liu, L. Z. Zheng, *Chem. J. Chinese U.* 34 (2013) 551.
26. Y. Ma, X. L. Shen, Q. Zeng, L. S. Wang, *Microchim. Acta*, 184 (2017) 4469.
27. Y. Liu, J. Liu, J. Liu, W. Gan, B. Ye, Y. Li, *Microchim. Acta*, 184 (2017) 1285.
28. A.J.S. Ahammad, A.A. Shaikh, N.J. Jessy, T. Akter, A.A. Mamun, P.K. Bakshi, *J. Electrochem. Soc.*, 162 (2015) B52.
29. H. J. Chen, Z. H. Zhang, D. Xie, R. Cai, X. Chen, Y. N. Liu, S. Z. Yao, *Electroanalysis*, 24 (2012) 2109.
30. A. Salimi, B. Kavosi, F. Fathi, R. Hallaj, *Biosens. Bioelectron.*, 42 (2013) 439.
31. D. M. Hawkins, D. Stevenson, S. M. Reddy, *Anal. Chim. Acta*, 542 (2005) 61.
32. H. Zhang, S. Shuang, L. Sun, A. Chen, Y. Qin, C. Dong, *Microchim. Acta*, 181 (2014) 189.
33. Z. Su, X. Xu, H. Xu, Y. Zhang, C. Li, Yan Ma, D. Song, Q. Xie, *Microchim. Acta*, 184 (2017) 1677.

34. Q. Wang, Z. Zhou, Y. Zhai, L. Zhang, W. Hong, Z. Zhang, S. Dong, *Talanta*, 141 (2015) 247.
35. B. Jeong, R. Akter, J. S. Choi, M. A. Rahman, *Electroanalysis*, 27 (2015) 2588.